3-24-2017

Focused Electron Beam Induced Deposition of Copper with High Resolution and Purity from Aqueous Solutions

Samaneh Esfandiarpour
University of Kentucky, samaneh.esfandiarpour@uky.edu

Lindsay Boehme
PowerTech Water, LLC

J. Todd Hastings
University of Kentucky, todd.hastings@uky.edu

Right click to open a feedback form in a new tab to let us know how this document benefits you.

Follow this and additional works at: https://uknowledge.uky.edu/ece_facpub

Part of the Electrical and Computer Engineering Commons, and the Nanoscience and Nanotechnology Commons

Focused Electron Beam Induced Deposition of Copper with High Resolution and Purity from Aqueous Solutions

PAPER

Focused electron beam induced deposition of copper with high resolution and purity from aqueous solutions

Focused Electron Beam Induced Deposition of Copper with High Resolution and Purity from Aqueous Solutions

Samaneh Esfandiarpour,[‡] Lindsay Boehme, [‡†] and J. Todd Hastings[*]

Electrical and Computer Engineering, University of Kentucky, Lexington, KY 40506

ABSTRACT: Electron-beam induced deposition of high-purity copper nanostructures is desirable for nanoscale rapid prototyping, interconnection of chemically synthesized structures, and integrated circuit editing. However, metalorganic, gas-phase precursors for copper introduce high levels of carbon contamination. Here we demonstrate electron beam induced deposition of high-purity copper nanostructures from aqueous solutions of copper sulfate. The addition of sulfuric acid eliminates oxygen contamination from the deposit and produces a deposit with ~95 at. % copper. The addition of sodium dodecyl sulfate (SDS), Triton X-100, or polyethylene glycole (PEG) improves pattern resolution and controls deposit morphology but leads to slightly reduced purity. High resolution nested lines with a 100 nm pitch are obtained from $CuSO_4-H_2SO_4-SDS-$

[‡] These authors contributed equally

[†] Currently at PowerTech Water, LLC, 145 Graham Ave, ASTeCC A205, Lexington, KY 40506

[*] Corresponding Author, E-mail: todd.hastings@uky.edu

H_2O. Higher aspect ratios (~1:1) with reduced line edge roughness and unintended deposition are obtained from $CuSO_4$–H_2SO_4–PEG–H_2O. Evidence for radiation-chemical deposition mechanisms was observed, including deposition efficiency as high as 1.4 primary electrons/Cu atom.

KEYWORDS: electron beam induced process, liquid phase, copper deposition, FEBID, direct write nanofabrication.

1. INTRODUCTION

Focused electron-beam induced deposition (FEBID) is a nano-scale patterning technique that allows the direct deposition of functional materials. This process has a variety of applications such as nano-scale rapid prototyping, lithographic mask and imprint template repair, interconnection to chemically synthesized nanostructures, and integrated circuit editing. Liquid-phase processes, in which deposition occurs at the interface between a substrate and a bulk liquid, are being investigated because they have potential for higher purity deposits, simpler precursors, access to new materials and faster processing rates. To date, Pt[1-3], Au[4], Ag[5-7], Pd,[8] bimetallic alloys (AuAg and AuPt)[9], semiconductors (CdS)[10] and Cu[11-12] have been successfully deposited in sealed liquid cells. Recently, liquid-phase FEBID (LP-FEBID) on bulk substrates without liquid cells was accomplished using in-situ injection,[7, 13] environmental SEM (ESEM), or a combination of the two.[14] Growth rates 10^5 times greater than standard gas-phase FEBID were reported for carbon deposition from a liquid phase process by Fisher *et al.*[7] However, there are challenges with this technique, such as the possibility of reactions in the bulk liquid, unintended deposition around the intended pattern, and liquid layer manipulation and control.

2

Due to its high electrical conductivity, copper is the primary material used to form the complex network of interconnects that provide the electrical wiring on an integrated circuit. Copper interconnects continue to shrink in size due to the miniaturization of the transistor; as a consequence, circuit edit and debugging are being implemented at the nano-scale. The ability to both etch and deposit high purity copper with an e-beam could provide a powerful tool for this purpose. EBID of copper was first demonstrated with gaseous organometallic precursors that introduced a large amount of impurities, primarily carbon, into the deposit.[15-17] Contaminant incorporation in copper can result in impaired grain growth,[18] accelerated electromigration failure,[19] and poor conductivity[20-21], all of which are detrimental for the microelectronics industry. Deposition from liquid precursors promises potential solutions to these issues.

Liquid-phase FEBID of copper has been recently demonstrated on bulk substrates using in-situ hydration of solid precursors in an ESEM [14] and using a capillary-style liquid injection system.[13] In both cases, aqueous solutions of copper sulfate served as the precursor. In the ESEM effort, a surfactant, sodium dodecyl sulfate, was added to the precursor solution to thin and stabilize the liquid film to obtain higher resolution. Significant oxygen contamination was observed in both cases, qualitatively by Randolph et al.[13] and estimated at 16-19 at.% by Bresin et al.[14] In the latter case sub-100 nm features were patterned, but no attempt was made to optimize the process for high resolution. Finally, unintended deposition, along with residue and precipitates, were often observed near the exposed patterns, and maintaining a stable, thin liquid layer through which one could pattern was challenging. Nevertheless, some preliminary measurements indicate that the resistivity of copper deposited from these solutions can be orders of magnitude lower than that deposited by gas-phase processes.[22]

The goal of this work was to improve the resolution and purity of copper FEBID from liquids while reducing unintended deposition and avoiding precipitation of undesired products. Figure 1 illustrates the deposition process used in this work in which the electron-beam reaches the substrate through a thin liquid layer and induces deposition at the interface. We hypothesized that the addition of sulfuric acid would reduce oxygen contamination by limiting copper oxides and hydroxides in the deposit. In addition, we expected both sulfuric acid and surfactants would improve pattern fidelity by reducing contact angles and stabilizing thin liquid films. Furthermore, additives common to electroplating baths should improve pattern fidelity by reducing grain size and by suppressing unintended deposition around the pattern. Finally, we anticipated that the low concentrations of organic additives would only slightly reduce the purity of the deposits. We found that these hypotheses were confirmed with varying degrees of quantitative improvement.
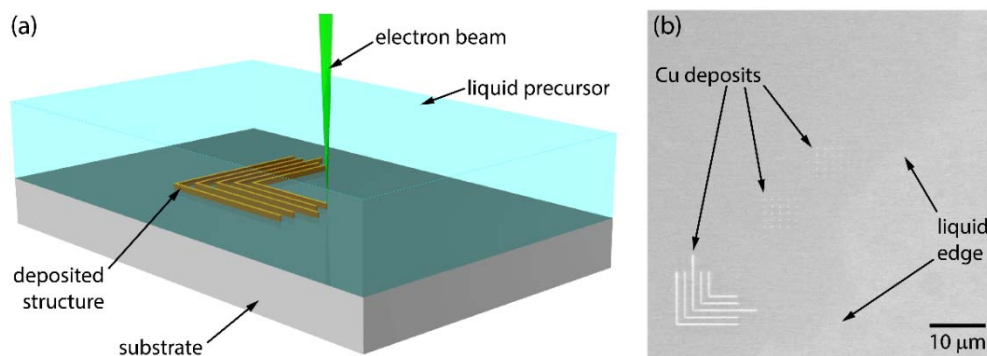

Figure 1. (a) Schematic of LP-FEBID of copper. An aqueous solution containing copper sulfate serves as the precursor and remains liquid in an environmental SEM. The electron-beam drives the deposition reaction at the substrate-liquid interface. (b) In-situ electron micrograph showing the liquid edge with deposited copper patterns. The liquid covered region is darker.

4

2. METHODS

All experiments were carried out in a Quanta 250 FEG environmental scanning electron microscope (ESEM, FEI Co., Hillsboro, OR, USA) at an accelerating voltage of 30 kV. Three different substrates were used: (1) a silicon substrate with a sputter deposited copper coating and polymer liquid wells, (2) a silicon substrate with a 1 μm thick electrodeposited copper film on a Mn/Cu-Ta-TaN barrier layer, and (3) a silicon substrate with a sputter deposited chromium coating. The sputtered coatings, both approximately 30 nm thick, improved adhesion of the deposits. The liquid wells were created using photolithography and SU-8 resist (Microchem Inc.). The SU-8 layer was 100 μm thick and the substrate was n-type silicon. The precursor was loaded into the well *ex-situ* as a dilute solution, dehydrated during ESEM pump down, and then rehydrated by control of water vapor pressure and substrate temperature. A liquid meniscus forms in the well with a thin central region in which high-resolution patterning can be conducted.

Substrates were oxygen plasma cleaned before each experiment and a Peltier stage was used to maintain their temperature during FEBID. Conductive silver paint (SPI Supplies) was used to attach the substrate to the sample mount. The precursor copper solution contained $CuSO_4:5H_2O$ (Fisher Scientific) in deionized water (DI H_2O). The solubility of copper sulfate at the temperatures of interest is 0.9 M, [23] but is reduced somewhat by the addition of sulfuric acid.[24] The concentration of $CuSO_4$ was initially chosen as 0.5 M to maximize the Cu^{2+} concentration without saturating the solution, but in most experiments it was reduced to 0.25 M to reduce unintended deposition as discussed in Section 3. Different solution compositions were studied; this included the addition of H_2SO_4 (EMD Millipore), surfactants, and plating additives, individually or in combination. Surfactants tested included: sodium dodecyl sulfate (SDS, Acros Organics) and Triton X-100 (Sigma-Aldrich). SDS was selected to test the effect of an anionic

surfactant, while Triton X-100 was selected to test the effect of a non-ionic surfactant. Additives tested included: Cl⁻ (KCl, Fisher Scientific), polyethylene glycol with a molecular weight of 1000 (PEG 1000, VWR), and bis-(3-sulfopropyl) disulfide (SPS, Combi-Blocks).

Prior to deposition, the substrate temperature was set to $3^{\circ}C$, a drop of the precursor copper solution was placed on the substrate (volumes noted in discussion), and the chamber was pumped to an initial pressure of 5.5 torr. At these conditions the precursor solution dehydrates to form either a solid, in the absence of H_2SO_4, or a viscous liquid, in the presence of H_2SO_4. By slowly increasing the water vapor pressure in the chamber to ~6 torr while maintaining the substrate temperature, the precursor rehydrates. The pressure can then be further adjusted to stabilize the droplet and establish a thin liquid edge for patterning.

Patterns were deposited using a Raith Elphy Plus electron beam lithography attachment and a fast beam blanker. The beam current was measured with a Faraday cup and Keithley 6487 picoammeter before each experiment. The beam current was between 365 and 386 pA for all experiments on the electrodeposited copper substrate. Patterns were deposited in the microwells at a beam current of 490 pA. Several patterns were used to test each solution: 100 nm, 200 nm, and 1 and 1.5 μm pitch nested lines with a linear dose of 5 to 30 μC/cm, dot arrays of 4 x 4 elements and 1 μm spacing with a dot dose of 100 pC, and 5 x 5 elements and 1 or 1.5 μm spacing with a dot dose of 100 to 1000 pC. Deposition efficiency was calculated from cross-sectional area estimates. Line widths were determined from top down SEM images by averaging over a 3 μm long segment that starts just inside the nested-L structure. Heights were determined from the same area using 60° tilt images. ImageJ was used for image calibrations and measurements.

3. RESULTS AND DISCUSSION

3.1. Copper Deposition from CuSO₄ and surfactants in microwells.

Sodium dodecyl sulfate (SDS) is a widely used anionic surfactant which will reduce the liquid contact angle with the substrate. Depositing copper in the thinner edge region of a droplet containing $CuSO_4$ and SDS improved pattern resolution compared to patterning in solutions containing only $CuSO_4$.[14] However, controlling the spreading of the droplet containing the surfactant can be challenging; thus, it is convenient to add microwells to the substrate to constrain the droplet as shown in Figure 2. These wells also allow different liquid precursors to be dispensed on the same substrate because hydration/condensation only occurs inside the wells and not on the top surface of the well material (SU-8 resist in this case).
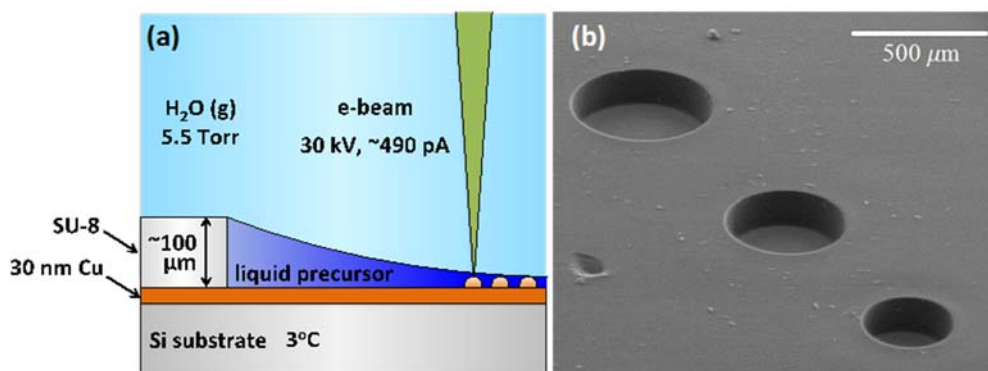
Figure 2.   (a) Schematic illustration of copper deposition from a liquid precursor in a micro-
well. (b) 50º tilt-view of SU-8 microwells with different diameters on a silicon substrate.

Figure 3 shows 400 nm pitch nested lines deposited from an aqueous solution of $CuSO_4$ and SDS, with initial concentrations of 0.25 M and 4 mM, respectively, in a 400-μm diameter well. The precursor was dehydrated on pump down and rehydrated in the ESEM chamber. There was some unintended deposition close to the patterning region. Moreover, precipitation of other solids was observed during the patterning process which is not surprising given the composition of the

7

solution and the experimental conditions. First, the temperature used for LP-FEBID is below the Krafft point for SDS (10°C),[25-27] such that micelles no longer form. Instead, if the concentration increases above the critical micelle concentration (~8 mM and only weakly dependent on temperature)[28] then SDS will precipitate as crystals. Secondly, $CuSO_4$ will slowly react with SDS to form $Cu(DS)_2$ which is essentially insoluble at the temperatures used here.[29]
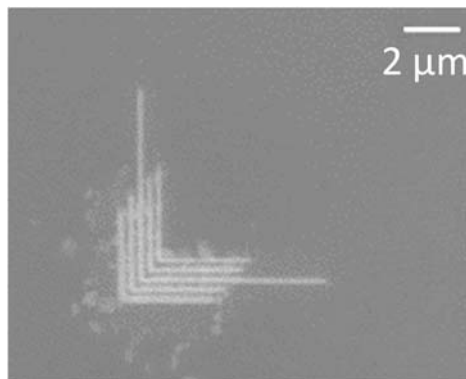
Figure 3.   400 nm pitch nested lines deposited in a micro-well from an aqueous solution with initial concentration of 0.25 M $CuSO_4$ and 4 mM SDS and a linear dose of 40 µC/cm.

Energy dispersive x-ray spectroscopy (EDX) measurements of these patterns showed carbon, oxygen, and sulfur peaks in addition to copper. Sulfur is either incorporated during deposition from the decomposition of SDS or stems from residual SDS or $Cu(DS)_2$ near the pattern. The concentrations were not quantifiable because of the proximity to the SU-8 well structure which contributed to the C and O signals and charged during the measurement. Thus, although SDS enables reasonably high resolution patterning, it appears to be a sub-optimal choice for copper FEBID under ESEM conditions.

To avoid problems associated with precipitation and reaction of SDS, it was replaced by Triton X-100. Triton X-100 is a common non-ionic surfactant which does not precipitate at low temperatures in aqueous solutions. Instead, lower operational temperatures are limited by freezing.[27]   In addition, Triton X-100 does not phase separate until it reaches its cloud point at

8

approximately 65°C. This broad range of working temperatures seems ideal for LP-FEBID. Figure 4(a) shows 1 μm pitch nested lines deposited from a solution with an initial concentration of 0.5 M $CuSO_4$ and 0.5 mM Triton X-100 at a dose of 40 μC/cm. Unwanted deposition and residues are visible surrounding the nested lines. The unwanted copper deposition was reduced when the initial concentration of $CuSO_4$ was decreased to 0.25 M (Figure 4(b)).
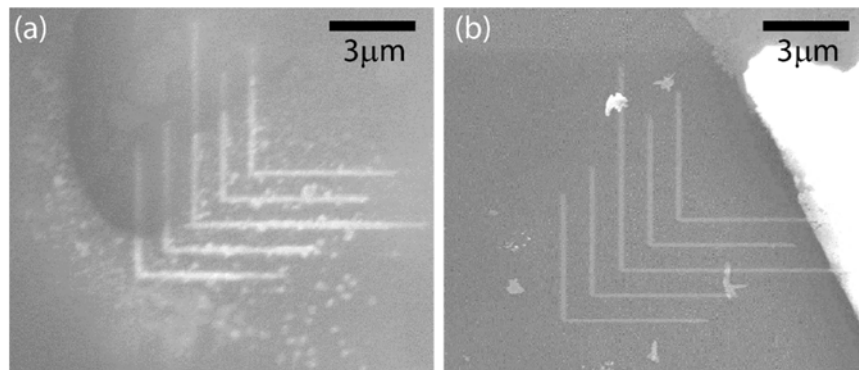
Figure 4.   Patterns deposited in microwells from an aqueous solution of $CuSO_4$ and Triton X-100. 1 μm nested lines were deposited at a dose of 40 μC/cm from a solution with initial concentrations of (a) 0.5 M $CuSO_4$ and 0.5 mM Triton X-100 and (b) 0.25 M $CuSO_4$ and 0.5 mM Triton X-100. Surfactant residue is visible in both images as dark regions covering the lines, and in (b) as a large, bright charged region on the right. Unintended copper deposition can be seen as bright spots in (a). Contrast and brightness were adjusted to make the various features as visible as possible.

Nevertheless, difficult to remove residues can also be seen in both experiments. One possible explanation for this is that Triton X-100 also has a hexagonal phase that can form an insoluble gel at high concentrations, even at room temperature.[31] Although this is reversible on heating in the presence of water, it is not likely to dissolve under the dehydrated and cooled ESEM conditions. Thus, Triton X-100–$CuSO_4$–H_2O solutions can only be used if the concentration is not allowed to enter the critical gel concentration range while in the ESEM, even during pump down. This can

prove challenging in the dynamic pressure environment of the ESEM. EDX measurements of these patterns revealed that there was no sulfur contamination after the replacement of SDS with Triton; however, significant oxygen content remained. Again, quantification was not possible for the small patterns in the microwells. Triton appears advantageous for avoiding precipitation and sulfur contamination, and conditions were found that produced little unwanted copper deposition. However, difficulties avoiding residue formation and continuing oxygen incorporation motivated a search for a further improved precursor solution.

3.2. Copper deposition from CuSO₄ and H₂SO₄

Sulfuric acid is a promising liquid reactant for use in reduced pressure environments such as an ESEM. First, it has a low vapor pressure of 10^{-3} Pa, [32] and has been used successfully under vacuum in an Auger spectroscopy system.[33] Secondly, the freezing point of the H_2SO_4-H_2O system falls rapidly toward 210 K as the H_2SO_4 concentration increases toward 5 M.[34] Likewise, concentration of the precursor can be controlled/estimated based on equilibrium with water vapor.[35] Previously, we exploited these properties to demonstrate electron beam induced etching (EBIE) of copper using H_2SO_4.[36]

Sulfuric acid is also a promising addition to solutions for liquid phase FEBID of Cu for several reasons. First, $CuSO_4$–H_2SO_4–H_2O is perhaps the most common system for copper electrodeposition and there is extensive guidance in the literature for choosing additives to control the morphology of the deposits. Secondly, $CuSO_4$ hydrates and precipitates rather abruptly as temperature falls and/or water vapor pressure rises. In contrast, sulfuric acid solutions remain liquid under most ESEM conditions and allow more gradual hydration/dehydration. Third, sulfuric acid reduces surface tension to improve wetting of the substrate and thin the liquid edge.

Fourth, adding sulfuric acid to the copper precursor solution is expected to prevent formation of copper oxides and copper hydroxide.

Despite the convenience of constraining the liquid precursor in microwells, the complications arising from quantification of deposit composition and the sporadic observance of resist residue prompted us to choose a more controlled substrate for further study. More data is provided in the supplementary information. In order to eliminate concerns about adhesion, interfacial layers, and charging we chose to deposit copper on thick electroplated copper on a silicon wafer as shown in Figure 5.
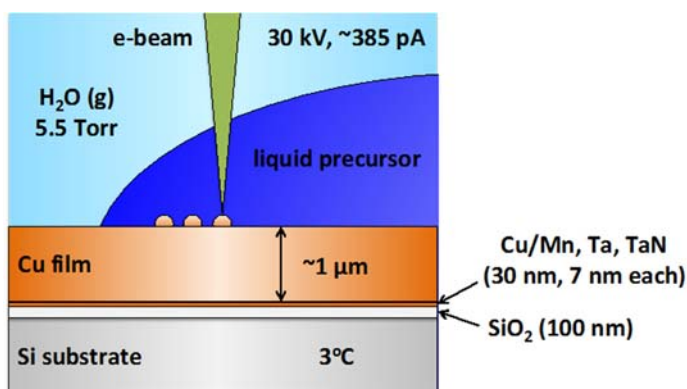
Figure 5.   Schematic of the experimental set-up for LP-FEBID of copper on an electrodeposited copper film.

At the concentration of acidic precursor tested, decreasing the dose helps to obtain cleaner patterns. However, higher resolution lines (200 nm and 100 nm pitch nested lines) were difficult to deposit from the acidic solution and the lines merged even with low doses. This may have occurred due to the droplet contact angle being too large, and the liquid edge not thin and uniform enough, for the electron beam to pattern high resolution lines. The region for depositing patterns successfully is only a few microns. The effect of liquid thickness is demonstrated in Figure 6 by incomplete 1-μm pitch nested lines in panel (a) and an incomplete 4 x 4 dot array with different

doses (200 pC, 300 pC and 400 pC from left to right) in panel (b). The desired pattern is missing close to the liquid edge due to the absence of the liquid, whereas, patterns were not deposited effectively in thicker liquid where the electron beam could not penetrate to the substrate.
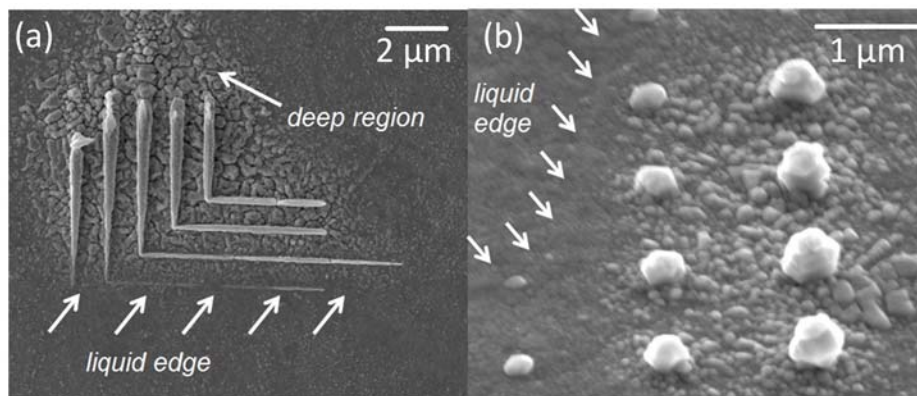

Figure 6.   Incomplete patterns deposited from 0.25 M $CuSO_4$ and 0.1 M H_2SO_4: (a) 1 μm pitch nested lines, (b) 45° tilted view of dot patterns with 4 x 4 elements and 1 μm pitch with increasing dose of 100 pC per dot for the columns from left to right.

3.3. Copper deposition from acidified $CuSO_4$ and surfactants

To overcome challenges associated with liquid thickness, surfactant was added to the precursor solution to reduce the interfacial energy. SDS was added to the solution described in the previous section and 0.25 μl of the new solution was dispensed onto the substrate. The substrate was then loaded into the ESEM with an initial temperature of 3ºC and pressure of 5.5 torr. After adjusting the chamber pressure and stabilizing the liquid edges, several patterns were deposited successfully. Figure 7 presents nested lines with (a) 100 nm pitch, (b) 200 nm pitch, and (c) 1 μm pitch deposited at a dose of 5 μC/cm from a $CuSO_4$, SDS, and H_2SO_4 solution on a copper substrate. Micrographs were taken *ex-situ* under high vacuum after rinsing the sample gently with DI-water. Addition of SDS to the acidified copper sulfate solution improved wetting behavior, providing a larger region

on the substrate surface for patterning at the droplet edge. However, as discussed for $CuSO_4$ and SDS, precipitation is seen in the background of the images.

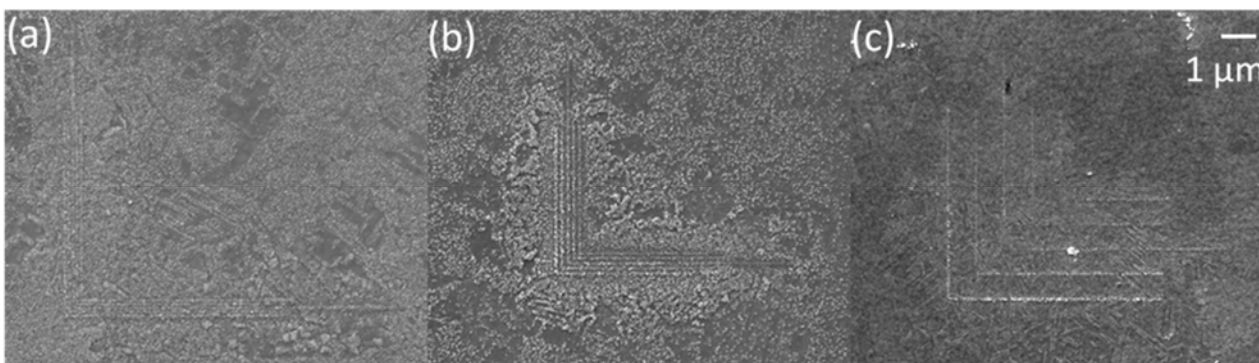Figure 7.   Nested lines with (a) 100 nm pitch, (b) 200 nm pitch, and (c) 1 μm pitch with a

dose of 5 μC/cm from 0.25 M $CuSO_4$, 1 mM SDS, and 0.1 M H_2SO_4 on a copper substrate.

Triton X-100 is known to be soluble and stable in acidic solutions, so it was added to the acidified $CuSO_4$ solution to reduce the contact angle and improve resolution while avoiding the precipitation and reactions present with SDS. Figure 8 shows 200 nm pitch nested lines with decreasing doses of (a) 20 μC/cm, (b) 10 μC/cm and (c) 5 μC/cm. Figure 9 displays a 60° tilted view of 5 x 5 dot arrays with 1 μm spacing. Here the dose effect is more easily observed – less copper is deposited at a lower dose. Unintended deposition between the elements decreases noticeably with dose from 1000 pC in (a) to 500 pC in (c). Moreover, the background is very clean compared to the previous precursor, SDS, which indicates that Triton X-100 is a better choice to improve the wetting process. Figure 8 and Figure 9 indicate that reducing the dose is likely lessening the unintended depositions close to the exposed region.
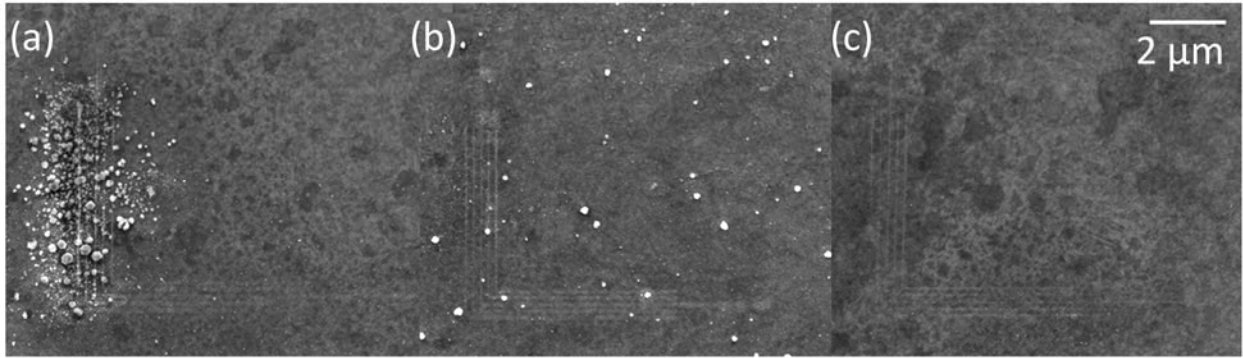
Figure 8.   200 nm pitch nested lines deposited from an aqueous solution of 0.25 M CuSO$_4$, 1 mM Triton X-100, and 0.1 M H$_2$SO$_4$ at a dose of (a) 20 µC/cm, (b) 10 µC/cm, and (c) 5 µC/cm on an electrodeposited copper film.
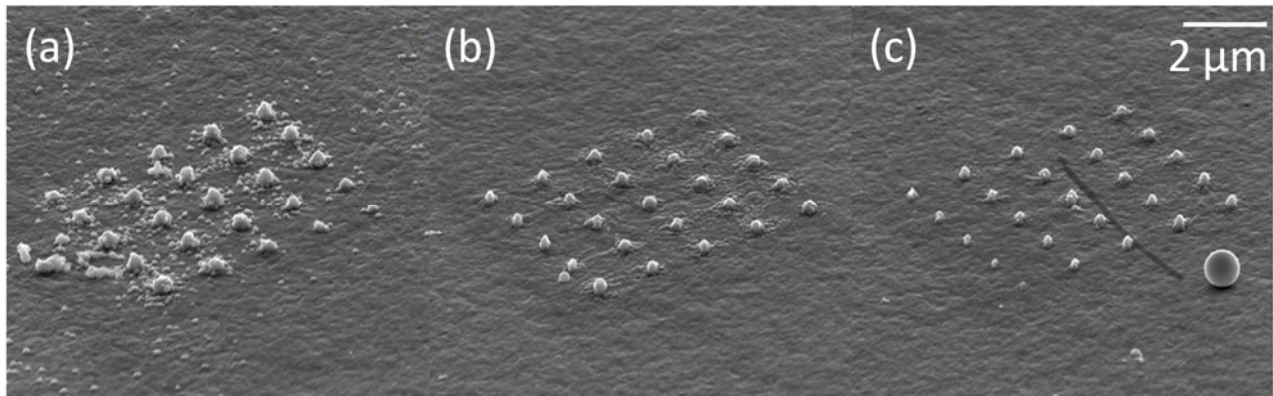
Figure 9.   60° tilt-view of dot arrays of 5 x 5 elements and 1 µm spacing deposited from an aqueous solution of 0.25 M CuSO$_4$, 1 mM Triton X-100, and 0.1 M H$_2$SO$_4$ at a dose of (a) 1000 pC, (b) 800 pC, and (c) 500 pC, per dot.

Figure 10 shows the reduction of unintended deposition by the addition of Triton X-100 to the acidified copper precursor. Panel (a) is a magnified view of 1 µm pitch nested lines deposited from CuSO$_4$-H$_2$SO$_4$ without additives at a dose of 30 µC/cm, panel (b) is the same pattern and dose after adding Triton X-100, and panel (c) is µm pitch nested lines from a CuSO$_4$, Triton X-100, and H$_2$SO$_4$ precursor at a lower dose of 20 µC/cm. The Triton X-100 reduces grain size and deposition

rate. It also appears to reduce, though certainly not eliminate, unwanted deposition around the desired patterns.

Figure 10. 1 μm nested lines deposited from an aqueous solution of (a) 0.25 M CuSO4 and 0.1 M H2SO4 at a dose of 30 μC/cm, (b) 0.25 M CuSO4, 1 mM Triton X-100, and 0.1 M H2SO4 at a dose of 30 μC/cm, (c) 0.25 M CuSO4, 1 mM Triton X-100, and 0.1 M H2SO4 at a dose of 20 μC/cm on an electrodeposited copper film.

3.4. Copper Deposition with Plating Additives

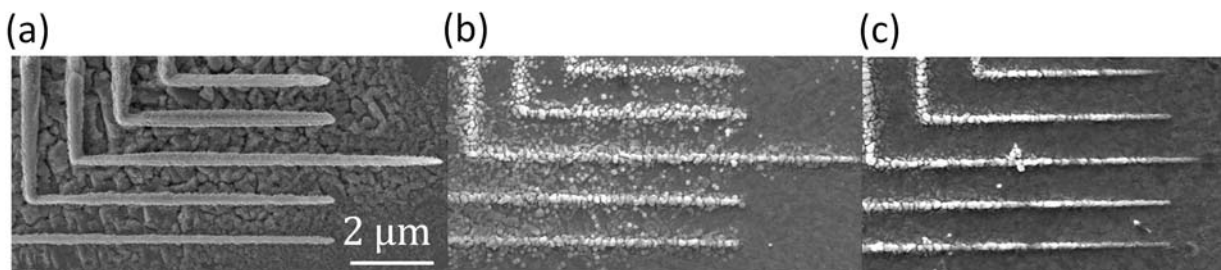Another approach to improve deposition was to borrow chemistries associated with electroplating or electrodeposition. Copper electrodeposition is widely used in the microelectronics industry for the fabrication of printed circuit boards (PCB) and interconnect metallization. The miniaturization of microelectronic devices poses a challenge for copper electrodeposition. In order to enable void-free fill of small features with high aspect ratios, special plating additives are required. Copper is electrodeposited from an acidic copper sulfate electrolyte containing a suppressor, typically a polyether such as polyethylene glycol (PEG), an anti-suppressor or accelerator, which is a sulfur-containing molecule such as bis-(3-sulfopropyl) disulfide (SPS), and a chloride ion.[37-38] Suppressors adsorb to the copper substrate and inhibit deposition, while anti-suppressors have the opposite effect and promote copper deposition. Anti-suppressors are also referred to as brighteners because they act to refine the copper grain

structure.[39] The additive distribution within a feature controls the local plating rates to prevent defects from forming.

By taking advantage of the inhibiting property of a suppressor and adding it to the copper precursor solution, we hoped to prevent unwanted deposition surrounding the exposed patterns. Additive selection was based on organic molecules used for the metallization of nano-scale features: the most commonly used suppressor, PEG, and anti-suppressor, SPS. Figure 11 shows copper deposition results for all additive combinations tested at a line dose of 30 μC/cm. In the presence of PEG with Cl⁻, copper deposition is inhibited; similar to what is expected in electrodeposition. In the presence of chloride ion, suppressors will adsorb more strongly to the substrate and inhibit deposition more effectively.[40] The tilted micrographs in Figure 12 show the influence of PEG and Cl⁻ on copper deposition more clearly. At the same line dose, the height of the line deposited with no additives, PEG, and PEG with Cl⁻ was approximately 390 nm, 230 nm, and 95 nm, respectively. Visibly PEG suppresses copper deposition, and is even more effective at doing so with the addition of Cl⁻. When SPS is added, the copper lines become more granular in appearance and there are more precipitates that adhere to the substrate that cannot be rinsed away. In the presence of all 3 additives (Cl⁻, PEG, and SPS), precipitation of salts or other compounds is exacerbated. SPS does not work well at the conditions tested and is unsuitable for FEBID of copper. The best resolution was obtained with the acidified copper sulfate solution in the presence of PEG.

Figure 11. 1.5 μm pitch nested lines deposited from an acidified copper sulfate solution at a
line dose of 30 μC/cm with the addition of different plating additives: (a) no additives, (b)
100 ppm PEG 1000, (c) 50 ppm Cl- and 100 ppm PEG 1000, (d) 50 ppm SPS, and (e) 50
ppm Cl-, 100 ppm PEG 1000, and 50 ppm SPS. The best resolution is obtained in the
presence of PEG, panel (b).
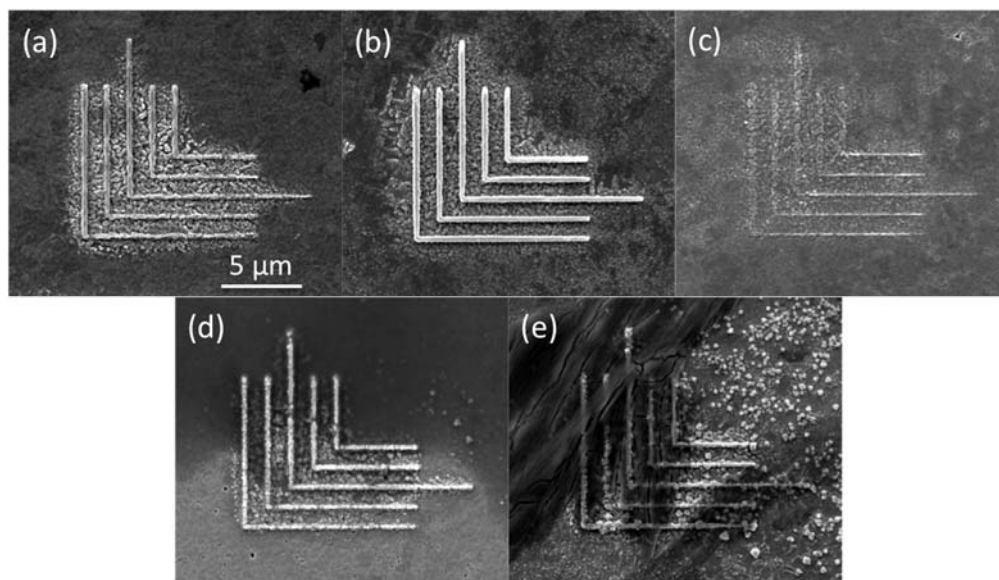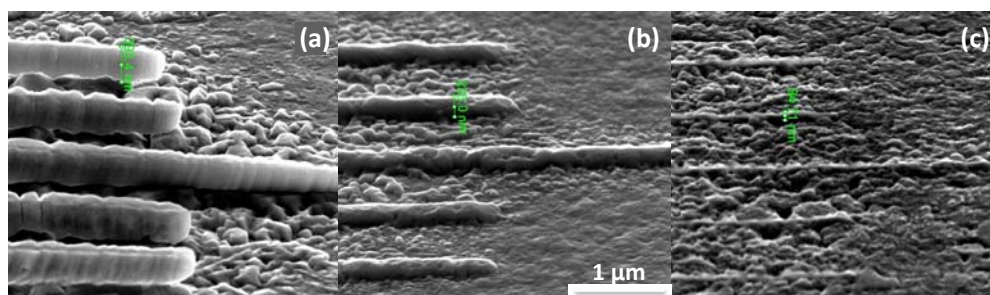

Figure 12. 1.5 μm pitch nested lines deposited from an acidified copper sulfate solution at a
line dose of 30 μC/cm with the addition of different plating additives: (a) no additives, (b)
100 ppm PEG 1000, and (c) 50 ppm Cl- and 100 ppm PEG 1000. Copper deposition is
suppressed in the presence of PEG, and even further with the addition of Cl-.

Figure 13 and Figure 14 show the effect of dose on 1.5-µm pitch nested lines for the acidified copper sulfate solution in the absence and presence of PEG, respectively. Both sets of data give similar results – thinner lines and less unintended deposition is observed at lower doses. The cleanest patterns are obtained at a dose of 5 µC/cm. At a dose below 5 µC/cm no deposition is visible. In Figure 15 we plot the estimated cross-sectional area of the primary deposit (excluding unintended deposition) vs. linear dose with and without PEG. The error bars represent the intra-experimental spread of the five line widths and account for proximity effects and liquid thickness variations. The error bars do not capture inter-experimental sources of error and this may explain the anomalously high cross-sectional area in the presence of PEG at 10 µC/cm period Regardless, as the dose increases the suppressive effect of PEG becomes clear. In addition, PEG markedly reduces the variation in linewidth, presumably because it creates a more uniform liquid layer and finer grained deposits. This effect is also qualitatively visible in Figure 14.

The relative uniformity of the unintended deposition in Figures 13 and 14 provides the opportunity to assess the range of this effect. We observe that the range is approximately 1µm which is consistent with the backscattered electron range at the surface of a silicon substrate with a 1µm thick copper film. Detailed description on the backscattered electron range is available in the supplementary document.

Finally, we can place approximate bounds on the efficiency of the deposition process. Based on the measurements from Figure 15, we can estimate the deposition efficiency in terms of Cu atoms deposited per primary electron. For the highest dose without PEG we find that approximately 1.4 primary electrons are required for each copper atom deposited. For the lowest dose, for which both solutions are similar, we find that 3.3 primary electrons per Cu atom are necessary. These numbers pertain only to the primary deposit, and the total efficiency will be higher if one includes

unintended deposition. The increase in efficiency at high doses in the absence of PEG is surprising as one would expect either linear growth or sub-linear growth depending on whether significant depletion of Cu^{2+} was occurring. Regardless, these efficiencies are markedly higher than Cu deposition from gas-phase metalorganic precursors. For example, when using copper(II) hexafluoroacetylacetonate, ~10 primary electrons are required for each deposited atom in the matrix (90 at.% carbon) and ~100 primary electrons required for each copper atom.[34]

Figure 16 shows the effect of dose and refresh time on 1.5 μm pitch 5 x 5 dot arrays from the same solution described above. As anticipated, more copper is deposited at a higher dose. Smaller copper dots are observed at 100 pC than 1000 pC, Figure 16 (a) and (b), respectively. To check if refresh time affects liquid-phase FEBID of copper, the dot array was deposited with a dose of 100 pC and pulsed 10 times to give a total dose of 1000 pC. A refresh time of 100 ms was added between each pulse. Comparing experiments with and without added refresh time, Figure 16 (c) and (b), respectively, there is little to no difference. Refresh time does not appear to have an effect on the FEBID of copper from these solutions, suggesting that no significant depletion of Cu^{2+} is occurring under the conditions investigated here.
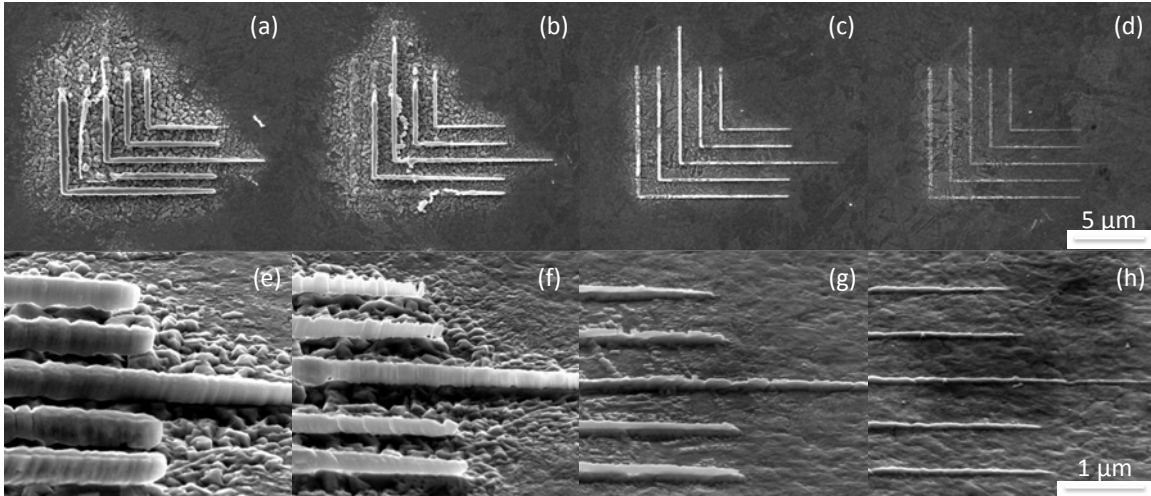
Figure 13. 1.5 μm pitch nested lines deposited from an acidified copper sulfate solution with decreasing line dose: (a) 30 μC/cm, (b) 20 μC/cm, (c) 10 μC/cm, and (d) 5 μC/cm. Panels (e-h) are 60° tilt micrographs of (a-d), respectively. Lines become thinner and less unintended deposition occurs as the dose decreases.

Figure 14. 1.5 μm pitch nested lines deposited from an acidified copper sulfate solution with the addition of 100 ppm PEG 1000 with decreasing line dose: (a) 30 μC/cm, (b) 20 μC/cm, (c) 10 μC/cm, and (d) 5 μC/cm. Panels (e-h) are 60° tilt micrographs of (a-d), respectively. Lines become thinner and less unintended deposition occurs as the dose decreases.
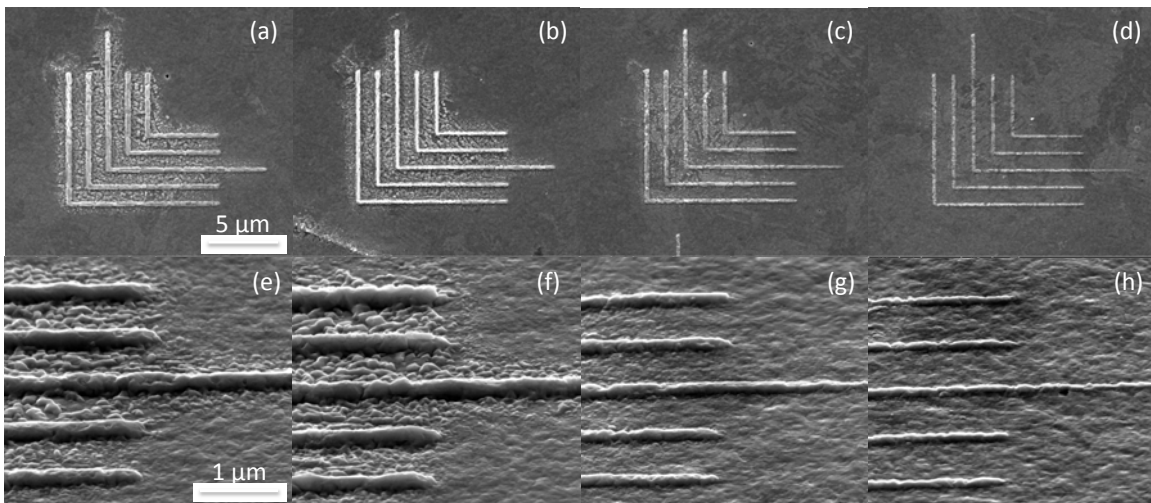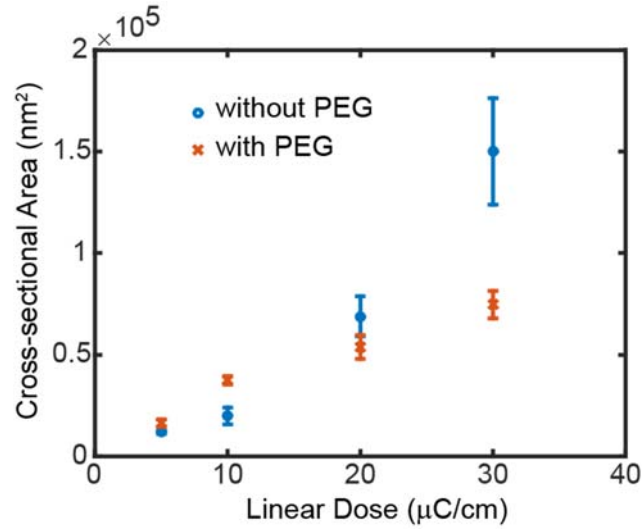
Figure 15. Cross-sectional area of deposited lines versus linear dose for the $CuSO_4$-H_2SO_4-H_2O system with and without 100 ppm PEG. The suppressive effect of PEG becomes clearly evident at higher doses, as does the reduction in the variation of linewidth.
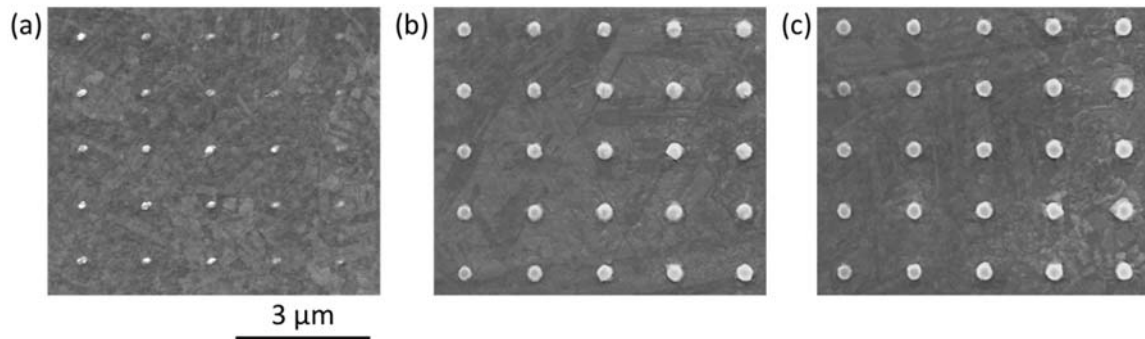
Figure 16. Dot arrays of 5 x 5 elements and 1.5 μm spacing deposited from an acidified copper sulfate solution with the addition of 100 ppm PEG 1000 at a dose of (a) 100 pC, (b) 1000 pC, and (c) 100 pC x 10 pulses with a refresh time of 100 ms, per dot. Deposition increases with dose and there is no observable effect when a refresh time is added.

Denser features were deposited to determine the highest resolution achievable. Deposition of 200 and 100 nm pitch nested lines from acidified copper sulfate with PEG 1000 are shown in Figure 17. The large spot at the center of the pattern in panel (a) was unintentional. The beam parked on

this nested line pattern during deposition at another location nearby. Regardless of the extra deposit, it is evident that the 200 nm pitch nested lines are well resolved. Pushing the resolution further to 100 nm pitch nested lines proves challenging (Figure 17 (b) and (c)). As the line width and spacing between each line approach one another, the deposited lines become nearly indistinguishable.
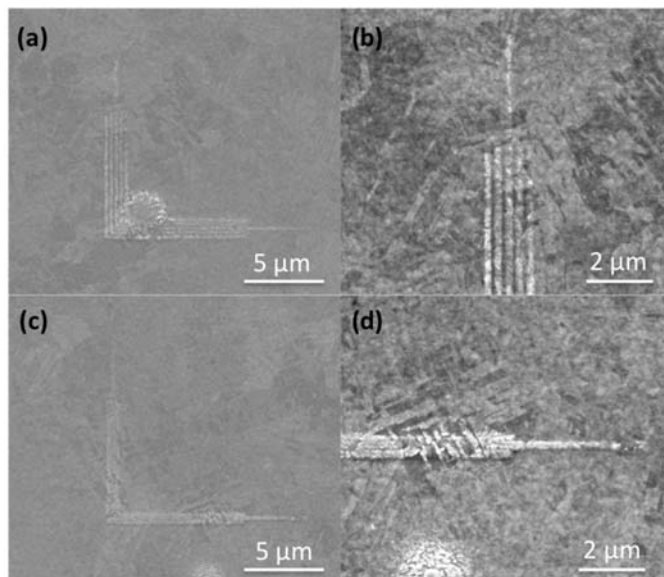
Figure 17. Nested lines deposited from an acidified copper sulfate solution at a line dose of 5 μC/cm with the addition of 100 ppm PEG 1000: (a) and (b) 200 nm pitch nested lines; (c) and (d) 100 nm pitch nested lines.

4. Composition and Purity of Copper Deposits

Liquid phase FEBID promises improved purity in comparison with the gas phase process. To quantify the purity of the deposits, energy dispersive x-ray spectroscopy (EDX) was performed on a large copper feature deposited from an acidified copper sulfate solution. This feature was deposited on a silicon substrate that had been sputter coated with 20 nm of chromium to improve adhesion, but the thickness of the feature eliminates almost any contribution from the substrate.

22

The EDX spectrum and a micrograph of the deposited material are shown in Figure 18, and a comparison of EDX elemental quantification is shown in Table 1. There is only a slight increase in the carbon content of the copper deposit, about 5 at. %, compared to the silicon reference. Moreover, no oxygen was detected in the deposit, which indicates significantly higher purity copper has been deposited in this process than from the $CuSO_4$−SDS solution. After correcting for the background carbon signal, the actual metal content is approximately 95 at. %, which is dramatically higher than reported values for Cu from gas FEBID deposited from hexafluoro-acetyl-acetonate copper vinyl-trimethyl-silane [41], copper(II) hexafluoroacetylacetonate [42] which was at most 11 at. % Cu, and recently copper deposited with FEBID from Cu(I) and Cu(II) precursors upon post-growth annealing[21] which was at most 12 ± 2 at. %. Deposits formed by irradiating cooled, condensed layers of copper(II) hexafluoroacetylacetonate in UHV showed similar low copper content as deposited, but could be significantly purified by subsequent exposure to atomic oxygen and atomic hydrogen.[35]
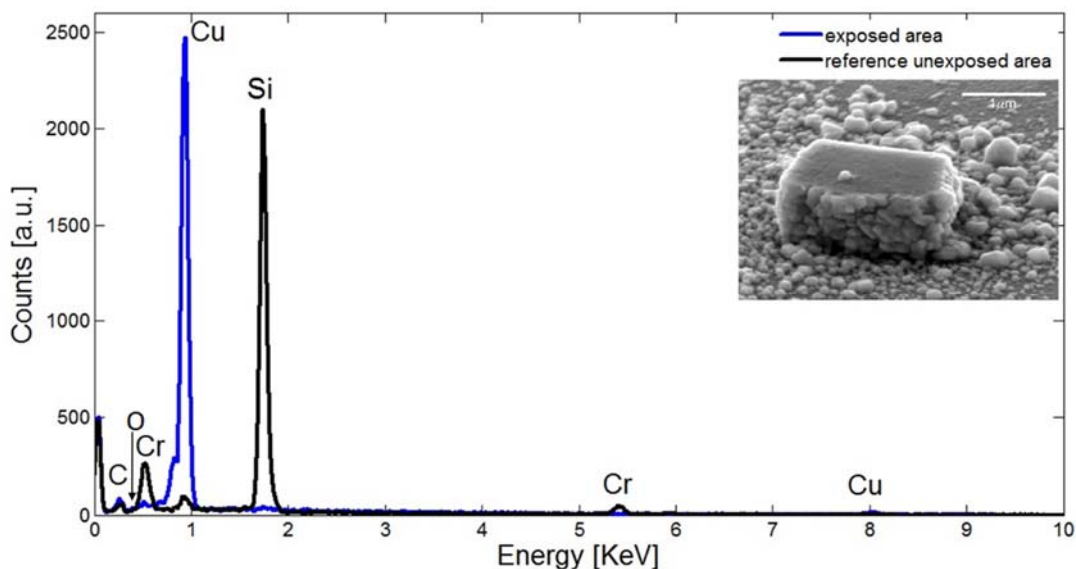
Figure 18. EDX spectra of copper deposits produced by LP-FEBID from acidified copper sulfate solution.

	C	O	Si	Cu
Si ref	8.1	0.49	91	-
Cu Deposits	12	-	0.60	88

EDX also reveals the copper deposits from the acidified copper sulfate solution with addition of PEG have more contamination than deposits with no additive in the mixture. An upper bound of 12 at.% carbon and 3 at.% oxygen was seen in the spectrum of the copper feature in comparison with the silicon reference. Copper purity of this deposit was measured to be approximately 85 at.%. Quantified elemental EDX data is presented in Table 2 and Figure 19 shows the spectrum data of the deposit compared with the bare substrate. The deposited copper features are also shown.

Figure 19. Energy dispersive x-ray spectra of deposits produced by LP-FEBID from $CuSO_4$, H_2SO_4, and PEG.

	C	O	Si	Cu
Si reference	8.2	0.49	91	-
Cu Deposits	20	2.4	-	78

5. Deposition Mechanisms

There is discussion in the literature as to the relative contributions of electrochemical and radiation chemical processes in LP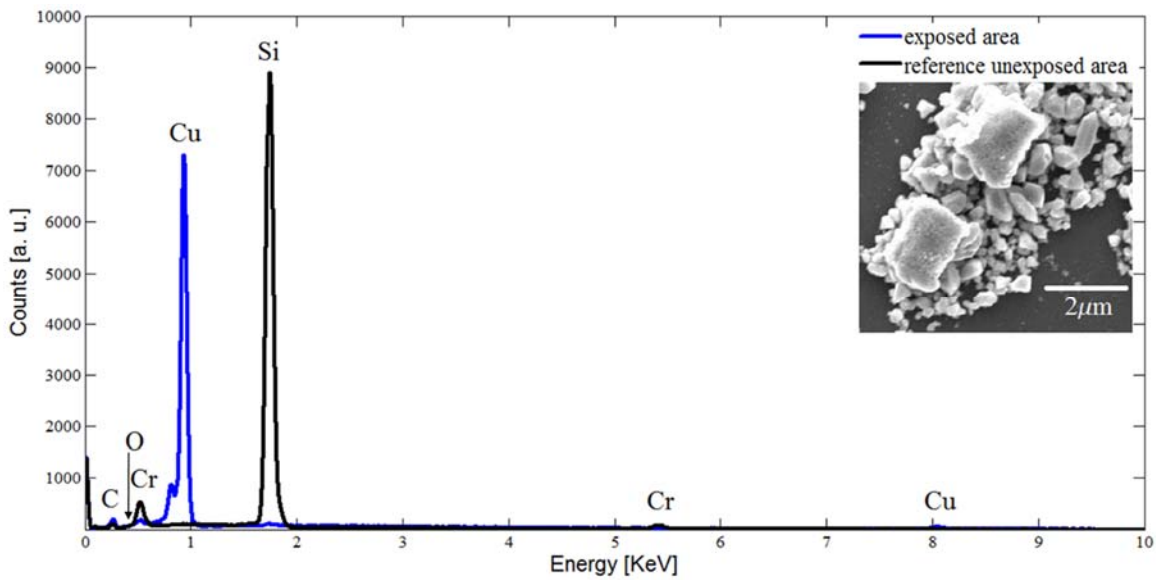-FEBID.[9,13,14,36,45] The reaction may be surface mediated, occurring in solution, or a combination of the two. In the first case, the e-beam is thought to create a localized virtual cathode on the substrate, thus enabling the electrodeposition of copper.[13] In this scenario, copper ions are reduced to copper metal at the interface by direct transfer of electrons. This deposition process proceeds according to the following half reaction.[43]

$$Cu_{(aq)}^{2+} + 2e^- \leftrightarrow Cu_{(s)} \ (E = 0.340 \ V)$$
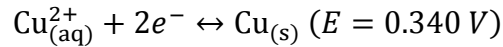
Alternatively, the reaction may be driven by radiation chemistry. In this case, a primary electron (e_{pr}^-) ionizes water and produces a secondary electron. This electron may ionize additional water molecules, or lose energy by other pathways until it becomes a solvated electron, $e^-(aq)$. The ionized water molecule subsequently produces a hydronium ion and a hydroxyl radical. The net reaction is

$$2H_2O \xrightarrow{e_{pr}^-} e^-(aq) + H_3O^+ + OH$$
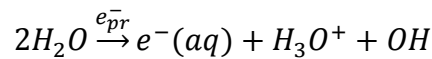
The solvated electron can directly reduce Cu^{2+} to Cu^{1+} $(k = 3 \times 10^{10} \ M^{-1}s^{-1})$ [44] and then Cu^{1+} to Cu(s). There is also an alternative pathway that may be important for acidic solutions. Specifically, the solvated electron can react with hydronium to form atomic hydrogen[44]

$$e^-(aq) + H_3O^+ \rightarrow H + H_2O \ (k = 2 \times 10^{10} \ M^{-1}s^{-1})$$
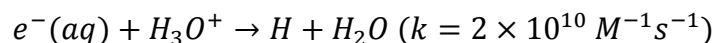
Atomic hydrogen can then serve as the reducing agent, though with a significantly slower reaction rate. [36]

$$Cu^{2+} + H \rightarrow Cu^{1+} + H^+ \ (k = 9 \times 10^7 \ M^{-1}s^{-1})$$
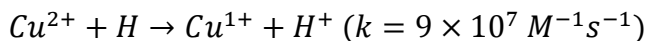
Of course, Cu^{1+} can also be reduced to metallic copper through the disproportionation reaction

$$Cu^{1+} + Cu^{1+} \rightarrow Cu(s) + Cu^{2+}$$

The deposit itself is built up by subsequent nucleation and growth from copper atoms or clusters.

The efficiency of copper deposition under some conditions (<1.4 primary electrons/Cu atom) suggests that a radiation-chemical mechanism likely contributes as a purely electrochemical mechanism would be limited to 2 primary electrons/Cu atom. In addition, Figure 20 shows 1 μm pitch nested copper lines on the electrodeposited copper film with additional evidence of copper reduction in solution. The first pa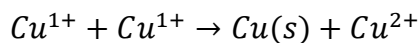ttern (a) is deposited from acidified copper sulfate solution and the second pattern (b) is deposited from the same solution with the addition of Triton X-100. Although there are clean patterns with sharp corners for the nested lines in both, there are two groups of patterns that have been deposited during the FEBID process at the same time; one on the substrate and the other in the solution. During the dehydration step, the pattern in the liquid floated away and re-deposited at a new location on the substrate. It should be noted that this double patterning was rarely observed, presumably because copper particles formed in solution did not create well-connected structures or because the secondary structure did not adhere to the substrate.
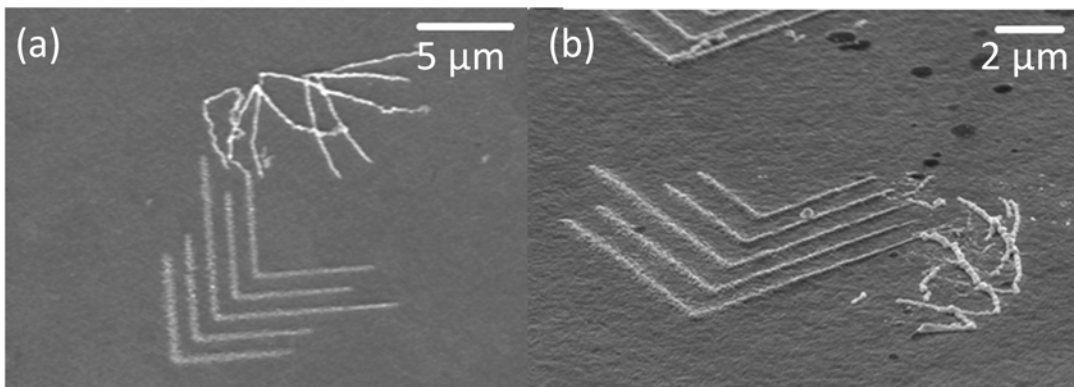
Figure 20. 1 μm nested lines on an electrodeposited copper film deposited from (a) acidified

copper sulfate solution and (b) acidified copper sulfate solution with Triton X-100 additive.

A second, distorted, copy of the pattern was observed nearby.

CONCLUSION

High purity copper can be deposited from aqueous solutions of copper sulfate, and deposition efficiencies greatly exceed those observed for metalorganic, gas-phase copper precursors. Addition of surfactants to these solutions enables dense, high resolution patterning (100 nm pitch nested-Ls) and increases the area available for deposition. This represents a significant improvement in the resolution of liquid-phase FEBID on bulk substrates. Previous efforts have only yielded < 100 nm features for isolated lines, [14] never for dense lines and spaces that truly reveal resolution. We found Triton X-100 is appropriate for the cooled experimental conditions in an ESEM, and it reduces precipitates and sulfur contamination compared to SDS. Sulfuric acid stabilizes the liquid films by decreasing the vapor pressure of the solutions; however, without surfactants, the substrate area available for direct writing only extends over a few microns.

Addition of Triton X-100 or PEG to the acidified copper sulfate solution thins the liquid film and produces finer grained structures. The highest resolution was obtained with Triton X-100 in acidified $CuSO_4$ while the highest aspect ratio structures were obtained with PEG in acidified $CuSO_4$. For the precursor solution studied here, thick, dense lines cannot be patterned without significant unintended deposition. Thus, until a means to mitigate this extra deposition is found, practical application of the technique will be limited to thin lines and/or low density patterns. EDX studies revealed that the purity of copper deposits from LP-FEBID is dramatically improved compared to the standard gas phase FEBID processes. Specifically, approximately 95 at.% copper

was deposited from acidic copper sulfate solution. Addition of PEG improved pattern fidelity, while only reducing the purity of the deposit to ~85 at.% which is still remarkably high for FEBID. The effects of additives were similar to those observed for electrodeposition of copper. However, significant evidence of radiation-chemical processes was also observed highlighting the complexity of the LP-FEBID process.

ACKNOWLEDGEMENTS

REFERENCES

1. Donev, E. U.; Schardein, G.; Wright, J. C.; Hastings, J. T., Substrate effects on the electron-beam-induced deposition of platinum from a liquid precursor. *Nanoscale* **2011,** *3* (7), 2709-17.

2. Donev, E. U.; Hastings, J. T., Electron-Beam-Induced Deposition of Platinum from a Liquid Precursor. *Nano Letters* **2009,** *9* (7), 2715-2718.

3. Donev, E. U.; Hastings, J. T., Liquid-precursor electron-beam-induced deposition of Pt nanostructures: dose, proximity, resolution. *Nanotechnology* **2009,** *20* (50), 505302.

4. Schardein, G.; Donev, E. U.; Hastings, J. T., Electron-beam-induced deposition of gold from aqueous solutions. *Nanotechnology* **2011,** *22* (1), 015301.

5. Ocola, L. E.; Joshi-Imre, A.; Kessel, C.; Chen, B.; Park, J.; Gosztola, D.; Divan, R., Growth characterization of electron-beam-induced silver deposition from liquid precursor. *Journal of Vacuum Science & Technology B* **2012,** *30* (6).

6. Bresin, M.; Nehru, N.; Hastings, J. T. In Focused electron-beam induced deposition of plasmonic nanostructures from aqueous solutions, *Proc. SPIE 8613, Advanced Fabrication Technologies for Micro/Nano Optics and Photonics,* **2013**; pp 861306-861306-6.

7. Fisher, J. S.; Kottke, P. A.; Kim, S.; Fedorov, A. G., Rapid Electron Beam Writing of Topologically Complex 3D Nanostructures Using Liquid Phase Precursor. *Nano Letters* **2015,** *15* (12), 8385-8391.

8. Jesse, S.; Borisevich, A. Y.; Fowlkes, J. D.; Lupini, A. R.; Rack, P. D.; Unocic, R. R.; Sumpter, B. G.; Kalinin, S. V.; Belianinov, A.; Ovchinnikova, O. S., Directing Matter: Towards Atomic Scale 3D Nanofabrication. *ACS Nano* **2016**.

9.   Bresin, M.; Chamberlain, A.; Donev, E. U.; Samantaray, C. B.; Schardien, G. S.; Hastings, J. T., Electron-Beam-Induced Deposition of Bimetallic Nanostructures from Bulk Liquids. *Angew. Chem.-Int. Edit.* **2013,** *52* (31), 8004-8007.

10.   Bresin, M.; Nadimpally, B. R.; Nehru, N.; Singh, V. P.; Hastings, J. T., Site-specific growth of CdS nanostructures. *Nanotechnology* **2013,** *24* (50).

11.   Lai, S.-E.; Hong, Y.-J.; Chen, Y.-T.; Kang, Y.-T.; Chang, P.; Yew, T.-R., Direct-Writing of Cu Nano-Patterns with an Electron Beam. *Microsc. microanal.* **2015,** *FirstView*, 1-5.

12.   den Heijer, M.; Shao, I.; Radisic, A.; Reuter, M. C.; Ross, F. M., Patterned electrochemical deposition of copper using an electron beam. *Apl Materials* **2014,** *2* (2).

13.   Randolph, S. J.; Botman, A.; Toth, M., Capsule-free fluid delivery and beam-induced electrodeposition in a scanning electron microscope. *RSC Advances* **2013,** *3* (43), 20016-20023.

14.   Bresin, M.; Botman, A.; Randolph, S. J.; Straw, M.; Hastings, J. T., Liquid Phase Electron-Beam-Induced Deposition on Bulk Substrates Using Environmental Scanning Electron Microscopy. *Microsc. microanal.* **2014,** *20* (02), 376-384.

15.   Utke, I.; Luisier, A.; Hoffmann, P.; Laub, D.; Buffat, P. A., Focused-electron-beam-induced deposition of freestanding three-dimensional nanostructures of pure coalesced copper crystals. *Applied Physics Letters* **2002,** *81* (17), 3245-3247.

16.   Luisier, A.; Utke, I.; Bret, T.; Cicoira, F.; Hauert, R.; Rhee, S. W.; Doppelt, P.; Hoffmann, P., Comparative study of Cu precursors for 3D focused electron beam induced deposition. *Journal of the Electrochemical Society* **2004,** *151* (8), C535-C537.

17.   Bret, T.; Utke, I.; Gaillard, C.; Hoffmann, P., Periodic structure formation by focused electron-beam-induced deposition. *Journal of Vacuum Science & Technology B* **2004,** *22* (5), 2504-2510.

18. Hau-Riege, S. P.; Thompson, C. V., In situ transmission electron microscope studies of the kinetics of abnormal grain growth in electroplated copper films. *Applied Physics Letters* **2000,** *76* (3), 309-311.

19. Brongersma, S.; Vanstreels, K.; Wu, W.; Zhang, W.; Ernur, D.; D'Haen, J.; Terzieva, V.; Van Hove, M.; Clarysse, T.; Carbonell, L. In *Influence of copper purity on microstructure and electromigration*, Interconnect Technology Conference, 2004. Proceedings of the IEEE 2004 International, IEEE: 2004; pp 45-47.

20. Szkudlarek, A.; Vaz, A. R.; Zhang, Y. C.; Rudkowski, A.; Kapusta, C.; Erni, R.; Moshkalev, S.; Utke, I., Formation of pure Cu nanocrystals upon post-growth annealing of Cu-C material obtained from focused electron beam induced deposition: comparison of different methods (vol 6, pg 1508, 2015). *Beilstein Journal of Nanotechnology* **2015,** *6*, 1935-1936.

21. Szkudlarek, A.; Vaz, A. R.; Zhang, Y. C.; Rudkowski, A.; Kapusta, C.; Erni, R.; Moshkalev, S.; Utke, I., Formation of pure Cu nanocrystals upon post-growth annealing of Cu-C material obtained from focused electron beam induced deposition: comparison of different methods. *Beilstein Journal of Nanotechnology* **2015,** *6*, 1508-1517.

22. A. Syam, Amjda; Hastings, J. Todd. "Electron-Beam Induced Deposition of Highly Conductive Copper Nanowires from Bulk Liquids," 60th International Conference on Electron, Ion, and Photon Beam Technology and Nanofabrication (EIPBN), **2016**.

23. Weast, Robert C., Melvin J. Astle, and William H. Beyer. CRC handbook of chemistry and physics. Vol. 69. Boca Raton, FL: CRC press, **1988**.

24. Holler, Homer Denison, and Elmer Line Peffer. "The relation between composition and density of aqueous solutions of copper sulphate and sulphuric acid." Journal of the Franklin Institute 181.4 (**1916**): 568.

25. Fontell, K., Liquid crystallinity in lipid-water systems. *Molecular Crystals and Liquid Crystals* **1981,** *63* (1), 59-82.

26. Nakayama, H.; Shinoda, K.; Hutchinson, E., The Effect of Added Alcohols on the Solubility and the Krafft Point of Sodium Dodecyl Sulfate. *The Journal of Physical Chemistry* **1966,** *70* (11), 3502-3504.

27. Kekicheff, P.; Grabielle-Madelmont, C.; Ollivon, M., Phase diagram of sodium dodecyl sulfate-water system: 1. A calorimetric study. *Journal of colloid and interface science* **1989,** *131* (1), 112-132.

28. Mukerjee, P.; Mysels, K. J. *Critical micelle concentrations of aqueous surfactant systems*; DTIC Document: 1971.

29. Orphanou, M.; Leontidis, E.; Kyprianidou-Leodidou, T.; Koutsoukos, P.; Kyriacou, K. C., Study of copper sulfide crystallization in PEO-SDS solutions. *Langmuir* **2004,** *20* (13), 5605-12.

30. Ahir , S. V., P. G. Petrov, and E. M. Terentjev. "Rheology at the phase transition boundary: 2. Hexagonal phase of Triton X100 surfactant solution. Langmuir **2002,** 18 (24), 9140-9148.

31. Ng, S. C.; Teh, H. C.; Hosea, T. J. C.; Gan, L. M., A Brillouin scattering study if the sol-gel transition in triton X-100-water systems. *Physics Letters A* **1984,** *105* (3), 153-156.

32. Jaeckervoirol, A.; Ponche, J. L.; Mirabel, P., Vapor-Pressures in the Ternary-System Water Nitric-Acid Sulfuric-Acid at Low-Temperatures. *J Geophys Res-Atmos* **1990,** *95* (D8), 11857-11863.

33. Fairbrother, D. H.; Johnston, H.; Somorjai, G., Electron Spectroscopy Studies of the Surface Composition in the H_2SO_4/H_2O Binary System. *The Journal of Physical Chemistry* **1996,** *100* (32), 13696-13700.

34. Zeleznik, F. J., Thermodynamic properties of the aqueous sulfuric acid system to 350 K. *Journal of physical and chemical reference data* **1991,** *20* (6), 1157-1200.

35. Massucci, M.; Clegg, S. L.; Brimblecombe, P., Equilibrium vapor pressure of H_2O above aqueous H_2SO_4 at low temperature. *J Chem Eng Data* **1996,** *41* (4), 765-778.

36. Boehme, L.; Bresin, M.; Aurélien, B.; James, R.; Hastings, J. T., Focused electron beam induced etching of copper in sulfuric acid solutions. *Nanotechnology* **2015,** *26* (49), 495301.

37. Andricacos, P. C.; Uzoh, C.; Dukovic, J. O.; Horkans, J.; Deligianni, H., Damascene copper electroplating for chip interconnections. *IBM Journal of Research and Development* **1998,** *42* (5), 567-574.

38. Boehme, L.; Landau, U., Rapid screening of plating additives for bottom-up metallization of nano-scale features. *Journal of Applied Electrochemistry* **2016,** *46* (1), 39-46.

39. Kondo, K.; Matsumoto, T.; Watanabe, K., Role of additives for copper damascene electrodeposition experimental study on inhibition and acceleration effects. *Journal of The Electrochemical Society* **2004,** *151* (4), C250-C255.

40. Hebert, K. R., Role of chloride ions in suppression of copper electrodeposition by polyethylene glycol. *Journal of The Electrochemical Society* **2005,** *152* (5), C283-C287.

41. Ochiai, Y.; Fujita, J. i.; Matsui, S., Electron-beam-induced deposition of copper compound with low resistivity. *Journal of Vacuum Science & Technology B* **1996,** *14* (6), 3887-3891.

42. Friedli, V.; Utke, I.; Mølhave, K.; Michler, J., Dose and energy dependence of mechanical properties of focused electron-beam-induced pillar deposits from Cu(C5HF6O2)2. *Nanotechnology* **2009,** *20* (38), 385304.

43. Bard, A. J.; Faulkner, L. R., *Electrochemical Methods: Fundamentals and Applications*. Wiley: **2000**.

44. Buxton, G. V.; Greenstock, C. L.; Helman, W. P.; Ross, A. B., Critical Review of rate constants for reactions of hydrated electrons, hydrogen atoms and hydroxyl radicals (·OH/·O− in Aqueous Solution. *Journal of Physical and Chemical Reference Data* **1988,** *17* (2), 513-886.

45. Unocic, R. R; Lupini, A. R.; Borisevich, A. Y.; Cullen, D. A.; Kalinina, S. V.; Jesse, S., Direct-write liquid phase transformations with a scanning transmission electron microscope. *Nanoscale* **2016**, 8, 15581-15588.